Pergamon

Geochimica et Cosmochimica Acta, Vol. 67, No. 18, pp. 3299–3311, 2003

0016-7037/03 $30.00 + .00

doi:10.1016/S0016-7037(00)01343-1

Adsorption of cadmium to *Bacillus subtilis* bacterial cell walls: A pH-dependent X-ray absorption fine structure spectroscopy study

M. I. Boyanov,[1,*] S. D. Kelly,[2] K. M. Kemner,[2] B. A. Bunker,[1] J. B. Fein,[3] and D. A. Fowle[3,†]

[1]Department of Physics, University of Notre Dame, Notre Dame, IN 46556, USA
[2]Environmental Research Division, Argonne National Laboratory, Argonne, IL 60439, USA
[3]Department of Civil Engineering and Geological Sciences, University of Notre Dame, Notre Dame, IN 46556, USA

(*Received May* 1, 2002; *accepted in revised form October* 22, 2002)

Abstract—The local atomic environment of Cd bound to the cell wall of the gram-positive bacterium *Bacillus subtilis* was determined by X-ray absorption fine structure (XAFS) spectroscopy. Samples were prepared at six pH values in the range 3.4 to 7.8, and the bacterial functional groups responsible for the adsorption were identified under each condition. Under the experimental Cd and bacterial concentrations, the spectroscopy results indicate that Cd binds predominantly to phosphoryl ligands below pH 4.4, whereas at higher pH, adsorption to carboxyl groups becomes increasingly important. At pH 7.8, we observe the activation of an additional binding site, which we tentatively ascribe to a phosphoryl site with smaller Cd-P distance than the one that is active at lower pH conditions. XAFS spectra of several cadmium acetate, phosphate, and perchlorate solutions were measured and used as standards for fingerprinting, as well as to assess the ability of FEFF8 and FEFFIT to model carboxyl, phosphoryl, and hydration environments, respectively. The results of this XAFS study in general corroborate existing surface complexation models; however, some binding mechanism details could only be detected with the XAFS technique.

1. INTRODUCTION

Discerning the chemical controls on metal transport in the environment is a prerequisite for understanding the fate of contaminants as well as for designing effective and efficient remediation strategies. Aqueous metal cations are exposed to mineral and biologic surfaces that affect their mobility in the subsurface; therefore, interaction with both must be well understood. Studies of metal adsorption onto mineral surfaces have been conducted for a wide variety of aqueous metals and environmentally important minerals. X-ray absorption spectroscopy has provided information about the mineral surfaces, binding sites, and the surface complexation reactions that occur at the mineral–water interface (Brown, 1990; Spadini et al., 1994; Sery et al., 1996; Venema et al., 1996; Farquhar et al., 1997; O'Day et al., 1998; Collins et al., 1999; O'Day, 1999; Randall et al., 1999). Substantially less is known about the mechanisms of biosorption. (For recent reviews, see Fein, 2000; Warren and Haack, 2001). Laboratory and field studies have demonstrated that bacterial cell walls efficiently adsorb a variety of aqueous metal cations (Beveridge and Murray, 1976, 1980; Beveridge and Koval, 1981; Crist et al., 1981; Harvey and Leckie, 1985; Goncalves et al., 1987; Konhauser et al., 1993). Therefore, it is likely that bacterial adsorption reactions can significantly affect metal contaminant transport and distribution in aqueous systems. A large portion of the bacterial adsorption data has been modeled by using a bulk partitioning approach, wherein a bulk partition coefficient is determined for the bacterial species of interest under fixed experimental conditions. This approach does not require a detailed understanding of the surfaces or of the adsorption mechanisms involved, but the applicability of the derived coefficient is limited to the conditions at which it was determined. Partition coefficients vary significantly as a function of pH, fluid composition, bacterial concentration, etc. (Bethke and Brady, 2000; Koretsky, 2000). Conversely, surface complexation models, which apply the formalism of aqueous ion association reactions to solute adsorption onto surfaces, are more flexible. Equilibrium constants can be determined for environmentally important adsorption reactions that are isolated in the laboratory. These constants can then be combined with other individually determined constants into a computational geochemical model of a complex system that has not been studied in the laboratory. Although in some cases workable surface complexation models can be obtained without exact assignment of the surface sites, the accuracy of these models increases with more precise identification of the adsorption mechanisms.

Fein et al. (1997) used a surface complexation approach to model metal adsorption onto the cell walls of *Bacillus subtilis*, an aerobic gram-positive bacterium. They employed acid/base titrations to determine acidity constants and site concentrations for the major surface functional groups, and they used bulk metal adsorption experiments to determine site-specific thermodynamic stability constants for the different surface complexes involved in metal adsorption. The acidity of the functional groups was modeled according to the following reaction stoichiometry:

$$R - AH^\circ \Leftrightarrow R - A^- + H^+ \quad (1)$$

Here, R denotes the bacterium to which each functional group type, A, is attached. The equilibrium between protonated and deprotonated sites is quantified with the corresponding equilibrium constant:

$$K_A = [R - A^-]a_{H+} \exp(\Delta Z\, F\, \Psi/RT)/\,[R - AH^\circ] \quad (2)$$

Here, the brackets represent concentration in moles of sites per

* Author to whom correspondence should be addressed (mboyanov@nd.edu).
† *Present address:* University of Windsor, Windsor, ON N9B, Canada.

Table 1. Compositions of the aqueous solution standards (mol L^{-1}).

Sample description	Cd	CH_3COO[a]/ PO_4[b]	H_2O	NH_4[a]/ H[b]	[c]N_{bound}
$Cd(ClO_4)_2$	—[d]	—	—	—	0.00
$Cd:PO_4$ = 1:5	1.00	5.00[b]	41.68	13.0[b]	0.95[e]
$Cd:PO_4$ = 1:100	0.10	10.00[b]	28.50	9.93[b]	—
$Cd:CH_3COO$ = 1:10	0.05	0.50[a]	53.74	0.40[a]	1.35[f]
$Cd:CH_3COO$ = 1:2	2.00	4.00[a]	43.56	0.00[a]	1.70[g]
$Cd:CH_3COO$ = 1:4	1.00	4.00[a]	46.05	2.00[a]	2.60[g]
$Cd:CH_3COO$ = 1:100	0.05	5.00[a]	37.42	4.90[a]	2.90[h]

[a] For the acetate solutions.
[b] For phosphate solutions.
[c] N_{bound} is the calculated average number of ligands attached to the cadmium ion using equilibrium calculations.
[d] Samples with 0.05, 0.1, 0.15, and 0.2 M Cd were measured and found to be identical.
[e] As calculated by Caminiti (1982).
[f] Calculated with stability constants from Sillen and Martell (1971).
[g] As calculated by Caminiti et al. (1984a).
[h] Calculated with stability constants from Caminiti et al. (1984a).

kilogram of solution, and *a* represents the aqueous activity. ΔZ is the change in the charge of the surface species in the reaction; Ψ is the electric potential associated with the bacterial surface; T is absolute temperature, and F and R are Faraday's and the gas constants, respectively. Similar reactions can be used to model aqueous metal adsorption. Fein et al. (1997) reported that three types of binding sites, with pK_A (negative logarithm of K_A) values of 4.8, 6.9, and 9.4, were necessary to yield a satisfactory fit to the titration data for *B. subtilis*. They ascribed these values to carboxyl, phosphoryl, and hydroxyl functional groups, respectively, on the basis of known deprotonation constants for aqueous organic acids. It was also demonstrated that successful modeling of Cd adsorption data requires a model that accounts for binding to two different types of surface sites in the 2.0 to 8.0 pH range. These conclusions were based only on the titration studies and the pH dependence of the Cd adsorption, and not on a direct structural investigation. Martinez and Ferris (2001) invoke three binding sites for Cd on *B. subtilis*, under similar experimental conditions to those studied by Fein et al. (1997), to account for their ion selective electrode measurements of Cd^{+2} concentrations.

The objective of this X-ray absorption fine structure (XAFS) study is to determine directly the local environment of Cd adsorbed to *B. subtilis* cell walls as a function of pH. XAFS spectroscopy has the ability to determine atom types and numbers in the near vicinity of the atom whose absorption spectrum is being measured, as well as the distance of these atoms from the absorber. The main advantages of XAFS that make it one of the few structural methods applicable to natural and hydrated samples are as follows: the technique has elemental selectivity by tuning to the absorption edge of interest; no long-range (crystalline) order in the sample is required; and measurements are performed on the "as prepared" samples (i.e., no drying or ultrahigh vacuum environment is necessary). The local structural information obtained from those measurements and from spectra of appropriately chosen, well-characterized standards enable identification and quantification of the functional groups responsible for the bacterial surface complexation, thereby providing a rigorous test of the adsorption model. XAFS has been used previously to address metal speciation in lichens (Sarret et al., 1998a) and whole cells of microbes (Panak et al., 2000, 2002; Hennig et al., 2001; Webb et al., 2001), and to determine the binding mechanism in isolated fungal cell walls (Sarret et al., 1998b). The method has been applied to metal speciation in root and plant biomass (Salt et al., 1995, 1997; Kramer et al., 1996; Sarret et al., 2001) and humic substances (Xia et al., 1997a,b, 1998, 1999). The current study isolates and identifies the binding mechanism of Cd to the bacterial cell wall over a range of pH values. To our knowledge, the only similar study on bacteria to date is of uranyl adsorption onto *B. subtilis* at low pH (Kelly et al., 2001b).

2. MATERIALS AND METHODS

Detailed preparation and characterization procedures for *B. subtilis* cells can be found elsewhere (Fein et al., 1997, 2001). Cells were harvested during stationary growth phase, and were washed first in 0.1 mol/L $NaClO_4$ electrolyte, followed by a rinse with 0.03 mol/L HNO_3, and five rinses in fresh 0.1 mol/L $NaClO_4$ electrolyte. Washed bacteria were suspended in 0.1 mol/L $NaClO_4$ electrolyte to form a parent solution of 10 g (wet weight) bacteria L^{-1}. Six samples were prepared, into which appropriate amounts of dissolved metal were added from an aqueous 1000 ppm Cd standard to attain a final Cd concentration of 30 ppm. The pH was adjusted with 1.0 N NaOH or HNO_3. After the samples were allowed to equilibrate, the final pH was recorded, with final pH values being 3.4, 4.4, 5.5, 5.9, 6.4, and 7.8. Formation of Cd hydrolysis complexes is negligible in this pH range (Baes and Mesmer, 1973). The solutions were centrifuged, the supernatant was removed, and the resulting homogenous pastes were loaded into slotted Plexiglas holders and covered with Kapton film.

The XAFS spectrum taken from a sample reflects the average local environment of all probed atoms in it. To be able to separate, identify, and quantify the binding mechanism of Cd in the multiple binding-site case of the biomass requires a clear understanding of the isolated contributions in the spectra from all potential ligands. Gram-positive bacteria, such as the species used in this study, possess a cell wall constructed of a polymer network of macromolecules such as peptidoglycan and teichoic acid. These molecules are rich in carboxylate, phosphoryl, hydroxyl (or phenolic), and amino functional groups (Beveridge and Murray, 1980). We examined a series of cadmium acetate and cadmium phosphate aqueous solutions as possible end-member analogues to the likely important binding sites on the bacterial cell wall, and we tested the ability of FEFF8 (Ankudinov et al., 1998) to model the observed binding in each case. Although we recognize that interactions of Cd with the cell-wall functional groups may differ from the interactions with similar aqueous anions, it is likely that near-neighbor and next-near-neighbor electrostatic and/or covalent interactions will be quite similar, provided that the structures of the functional groups is similar. Several of the solution compositions were chosen to match the compositions of samples that were previously characterized by X-ray scattering. For hydrated Cd, four cadmium perchlorate solutions of different concentrations were prepared; for Cd bound to carboxyl functional groups, four cadmium acetate aqueous solutions of dif-

Table 2. Fit results from the perchlorate and phosphate aqueous solutions

Shell	N	R(Å)	$\sigma^2(10^{-3}$ Å$^2)$	ΔE_0(eV)
		$Cd(ClO_4)_2$		
O →	6.0 ± 0.2	2.27 ± 0.01	8.7 ± 0.5	−1.8 ± 0.4
H →	2 × N_O	2.93 ± 0.05	14 ± 5	−1.8 ± 0.4
		Cd:PO_4 = 1:5		
O →	5.9 ± 0.2	2.26 ± 0.01	9.4 ± 0.5	−4.0 ± 0.4
H →	2 × (N_O − N_P)	2.95 ± 0.05	13 ± 8	−4.0 ± 0.4
P →	1.0 ± 0.4	3.41 ± 0.03	14 (±5)[a]	−4.0 ± 0.4
		Cd:PO_4 = 1:100		
O →	5.9 ± 0.2	2.26 ± 0.01	9.5 ± 0.5	−3.3 ± 0.4
H →	2 × (N_O − N_P)	2.96 ± 0.05	13 ± 8	−3.3 ± 0.4
P →	1.5 ± 0.3	3.42 ± 0.02	14 (±5)[a]	−3.3 ± 0.4

[a] σ^2 factor held fixed to the best-fit value in a simultaneous fit of the two phosphate solution standards and the pH 3.4 sample.

ferent concentrations and different Cd:acetate ratios were prepared; and for Cd bound to a phosphoryl ligand, two cadmium phosphate aqueous solutions of different concentrations and Cd:phosphate ratios were prepared. The exact compositions are given in Table 1. Reference to works reporting studies of some of the solutions by X-ray scattering and nuclear magnetic resonance is also summarized in Table 1. All of the solutions were prepared by dissolving the appropriate amount of salt (reagent quality from Alfa Aesar) in reverse-osmosis ultrapure water (18 MΩ) and diluting the solution to a known volume. To shift the equilibrium toward complexed Cd ions, phosphoric acid was added to the Cd phosphate solutions and ammonium acetate was added to the Cd acetate solutions without pH adjustment. Cd K-edge XAFS spectra were taken from all samples at the Materials Research Collaborative Access Team (MRCAT) undulator beamline at the Advanced Photon Source, Argonne National Laboratory (Segre et al., 2000). The incident energy was scanned by using the Si(111) reflection of the double-crystal monochromator in quick-scanning mode, with the beamline undulator tapered approximately 2 keV on the third harmonic. Harmonic rejection was achieved by reflection from a Pt mirror. Beam size was adjusted to approximately 0.7 by 0.7 mm. The incident beam intensity, monitored with an ion chamber filled with nitrogen, did not change by more than 15% over the scan range. Linearity tests (Kemner et al., 1994) indicated less than 0.3% nonlinearity for the experimental setup with 50% beam attenuation.

The biomass sample spectra were measured in fluorescence mode with a Stern-Heald type detector (Stern and Heald, 1979) filled with Kr gas. To minimize radiation exposure and to test for repeatability of the scans, data were taken on each sample from four to six different incident beam positions. A total of 12 to 30 extended XAFS (EXAFS) scans (depending on Cd concentration in the sample) were collected and averaged. In addition, quick X-ray absorption near-edge scans lasting 1 to 2 min each were collected at the beginning on each sample to check for the possibility of radiation damage. No changes were observed on this time scale.

The solution standards were measured in transmission mode. A potential problem with solution measurements is that the formation of bubbles during intense X-ray exposure adds to the experimental noise. In these measurements, the intensity of the X-ray beam was reduced slightly until no bubble formation was observed. Six scans at three different beam positions were taken for each sample and averaged. In all measurements, a Cd foil was used to calibrate monochromator energy.

The EXAFS spectroscopy technique uses the small periodic variations in the absorption coefficient above the absorption edge energy of an element of interest to extract information about the local environment of that atom. There are complete references on the subject such as Koningsberger and Prins (1988) and Stern and Heald (1983). Only a short description of this theory is given here.

The EXAFS of a powderlike sample with Gaussian disorder can be derived as follows (Koningsberger and Prins, 1988):

$$\chi(k) = \sum_i \frac{(N_i S_0^2) F_i(k)}{k(R_i + \Delta R_i)^2} \exp\left(-2k^2\sigma^2 - \frac{2(R_i + \Delta R_i)}{\lambda(k)} \right) \sin(2k(R_i + \Delta R_i) + \delta_i(k)) \quad (3)$$

The sum is taken over the scattering paths that the ejected electron wave traverses in the material before it returns to the absorber atom. Here k is the electron wave vector,

$$k = \sqrt{2m(\hbar\omega - E_0)/\hbar^2}, \quad (4)$$

where E_0 is the edge energy and $\hbar\omega$ is the incident photon energy; N_i is the multiplicity of the path; ${S_0}^2$ is the constant passive electron reduction factor; R_i is the half-path length; ΔR_i is a shift in distance; ${\sigma_i}^2$ is the relative mean square displacement of length of the path (EXAFS Debye-Waller factor, which differs from the X-ray diffraction Debye-Waller factor); $F_i(k)$ and $\delta_i(k)$ are the effective scattering amplitude and phase shift of the scattered electron, respectively; and $\lambda(k)$ is the mean free path of the photoelectron. Thus, $\chi(k)$ is a superposition of sinusoidal waves in k-space with frequency related to the length of the path, and a Fourier transform (FT) of XAFS data results in peaks at close to the half path-length distance. The contribution from multiple scattering paths can be neglected in most room temperature measurements because of disorder and thermal motion. For the remaining single-scattering events the half-path length is equal to the distance of the scattering atoms from the absorber; thus, $|\mathrm{FT}\ k^n\chi(k)|$ may look like a radial distribution function, but distances will be shifted slightly to smaller R values because of the electron phase shift $\delta_i(k)$. The amplitudes of these peaks will depend in part on N_i and ${\sigma_i}^2$, the number of atoms and the disorder in the shells for a single-scattering path, but they can also be influenced by constructive

or destructive interference of signals from neighboring shells. By comparing $|\mathrm{FT}\ k^n\chi(k)|$ of similar samples and observing a peak's amplitude increase or decrease, one can, in general, make qualitative conclusions about the numbers or disorder of the atoms at the corresponding distance. The real or imaginary part of the FT may also be compared, keeping in mind that contributions corresponding to the different scattering atoms combine linearly to produce the observed features. The final structural parameters are obtained from fits of the real and imaginary parts of FT[$k^n\chi(k)$] by using model-scattering amplitudes and phase shifts.

In current EXAFS analysis, the electron effective scattering amplitude $F_i(k)$ and phase shift $\delta_i(k)$ are calculated ab initio for a cluster of atoms and then calibrated by using appropriate standards with known structure. The calibrated $F_i(k)$ and $\delta_i(k)$ are then used in a fitting routine where the structural parameters N_i, ΔR_i, and σ_i^2 are varied until a best fit to the experimental data are achieved. The UWXAFS suite of programs (Stern et al., 1995), including ATOMS (Ravel, 2001), FEFF8 (Ankudinov et al., 1998), and FEFFIT (Newville et al., 1995), was used in this work. The known crystallographic structures of cadmium acetate dihydrate (Harrison and Trotter, 1972) and cadmium phosphate (Averbuch-Pouchot et al., 1973; Bigi et al., 1986) were used as a basis for calculating backscattering amplitudes and phase shifts by using FEFF8, for clusters similar to those found in the aqueous solutions of cadmium perchlorate (Ohtaki et al., 1974), cadmium acetate (Caminiti et al., 1984a), and cadmium phosphate (Caminiti, 1982). FEFFIT was used to find the structural parameters that fit the observed spectrum best. The goodness of fit is characterized by two parameters: the XAFS reliability factor R, which measures how close the fit is to the experimental data, and the reduced χ^2 factor χ^2_ν, which takes into account the number of floating parameters and noise in the data. A comparison of these values for different fitting scenarios allows for an evaluation of the validity of one fitting model over another. More information is given in the FEFFIT documentation (Newville et al., 1995).

The raw data scans were aligned by the reference foil data and averaged. The edge energies for the samples were chosen at the inflection point of the absorption edges, and background was removed by using standard procedures with AUTOBK (Newville et al., 1993).

3. RESULTS AND DISCUSSION

3.1. Solution Standards

A series of cadmium perchlorate solutions was studied to gain an understanding of the EXAFS data from a hydrated Cd ion. Previous X-ray scattering studies of similar samples identified an octahedral hydration shell around the Cd ion (Ohtaki et al., 1974; Caminiti et al., 1984b; Marcus, 1988; Ohtaki and Radnai, 1993). No perchlorate-Cd ion interactions were expected in the samples, because perchlorate is typically a weakly binding ion. Indeed, no change in the EXAFS was observed with concentration changes in the range 0.05 to 2.0 mol/L. The data were successfully fitted with a hydration sphere of six water molecules. The final fit values and paths used are in Table 2. The empirical S_0^2 value for this solution and powder CdO was found to be 1.03 ± 0.05; this value was fixed in all subsequent fits.

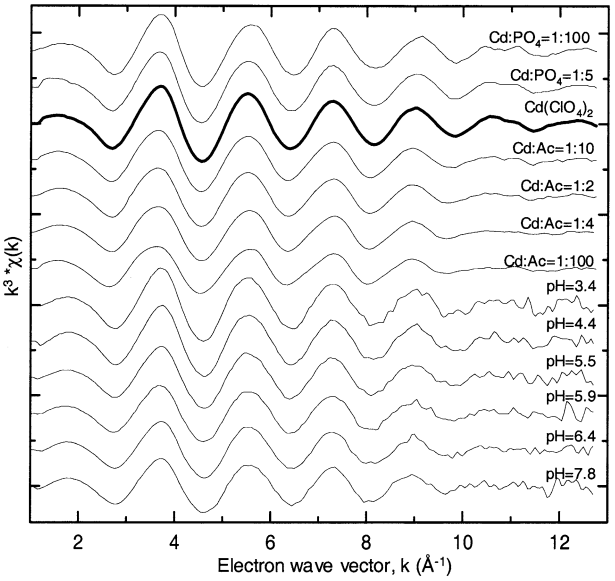

Fig. 1. k^3-weighted $\chi(k)$ data for the solution standards and biomass samples.

The data obtained for the solution standards are shown in Figure 1. Calculations based on published stability constants (Sillen and Martell, 1964, 1971) and measured for samples $Cd:CH_3COO$ = 1:2 and 1:4 (Caminiti et al., 1984a), indicate that Cd is complexed in the studied solutions. The calculated numbers of bound ligands are listed in Table 1. The results from the aqueous Cd studies suggested that complexation to a phosphate or carboxyl group involves substitution of one or more of the waters of hydration with the binding oxygen atom or atoms. Such inner-sphere complexation has been observed in X-ray scattering works on these and similar solutions (Caminiti and Johansson, 1981; Caminiti, 1982; Caminiti et al., 1984a,b). An increase in the disorder of the first hydration sphere, distance change, or a decrease in hydration number, are all possible results from complexation. This would affect the amplitude or position of the FT peak corresponding to that shell in the XAFS data, as discussed above. In addition, contribution from C or P atoms of bound carboxyl and phosphate groups, respectively, should be observed.

Figure 2 shows the magnitude of the transform, $|\mathrm{FT}\ k^3\chi(k)|$and, for a smaller distance range the imaginary part, $\mathrm{Im}[\mathrm{FT}\ k^3\chi(k)]$, of the perchlorate and two phosphate solutions. The spectra for the phosphate solutions are similar to the hydrated cadmium spectrum. A slight decrease in first-shell amplitude is observed, along with an increasing feature at 2.85 Å with the increase of phosphate:Cd ratio. The phosphate solution data were fitted with single scattering paths from a hydration shell at 2.3 Å and a P shell at 3.5 Å, and simultaneous data set and multiple k-weight fits were performed. Numerical results are in Table 2, and the quality of the fits is illustrated in Figure 3.

The attachment of a phosphate group preserves the number of oxygen atoms in the first coordination shell, but it increases the disorder slightly, as is seen by the increase in the O-shell σ^2 value. The number of P atoms is increased with increasing phosphate:Cd ratio, indicating that more Cd atoms are bound to

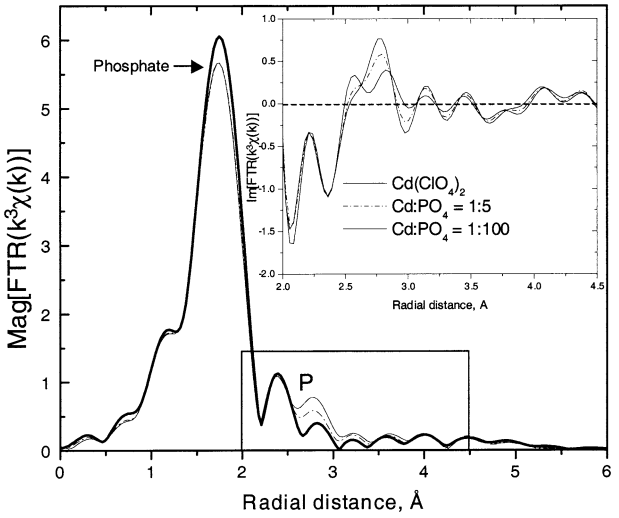

Fig. 2. Magnitude and imaginary part of FT[$k^3\chi(k)$] of the data for the Cd perchlorate and two Cd phosphate solutions. The contribution to the EXAFS signal from the P atom in the region 2.5 to 3.3 Å is noted.

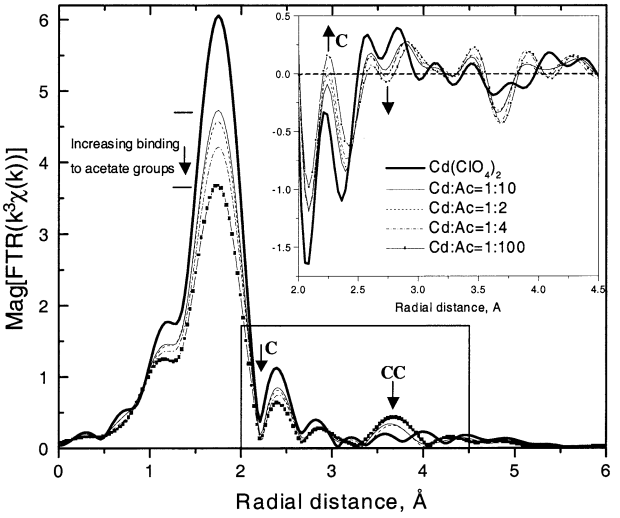

Fig. 4. Magnitude and imaginary part of FT[$k^3\chi(k)$] of the data for the Cd perchlorate and four Cd acetate solutions.

phosphate groups. Complexation constants are not available in the literature, so we could not compare the obtained coordination numbers. X-ray scattering studies on a solution identical to our Cd:PO_4 = 1:5 (Caminiti, 1982) determine a Cd-P distance of 3.5 Å and a Cd-P coordination of 0.95, which are close to the values we find in the fits. On the basis of the pH 0.7 to 1.0 of the solution and the H_3PO_4 and $H_2PO_4^-$ free radicals present at this pH, Caminiti (1982) suggests that the complexed species are $Cd(H_2O)_{6-x}(OPO_3H_2)_x^{+2-x}$. The Cd-P distance in crystal $Cd(H_2PO_4)_2 \cdot H_2O$ is also 3.5 Å (Averbuch-Pouchot et al., 1973). Thus, it is likely that Cd is bound to a diprotic phosphate group ($H_2PO_4^-$) in these solutions; however, lack of Cd-phosphate stability constants precludes exact speciation and the other possibilities cannot be excluded.

Figure 4 shows the magnitude |FT $k^3\chi(k)$| and, for a smaller distance range, the imaginary part Im[FT $k^3\chi(k)$], of the perchlorate and the four acetate solutions. A large reduction in first-shell amplitude relative to that of the hydrated Cd sample and a decreasing peak height at 2.3 Å of |FT $k^3\chi(k)$| occurs with increasing acetate:Cd ratio. Qualitative observation of Im[FT $k^3\chi(k)$] in the range 2.2 to 3.0 Å also reveals a feature that becomes more pronounced with increasing acetate:Cd ratio. The acetate solution data were fitted with single-scattering paths from a hydration shell at 2.3 Å and a C shell at 2.7 Å, and simultaneous, multiple k-weight fits were performed. The large decrease in the main peak amplitude is caused by the destructive interference between the contribution from the hydration shell and that of the C atom in the carboxyl group. Increased amplitude in the acetate samples relative to the hydrated Cd and the phosphate solutions is also noticeable in the range 3.5 to 4.0 Å. The data in this region of the FT were successfully modeled with collinear multiple scattering from the second, farther C atom in the acetate molecule, with the number of paths constrained to the number of closer C atoms. We do not observe that feature in the biomass spectra. Numerical results are in Table 3, and the quality of the fits is illustrated in Figure 5.

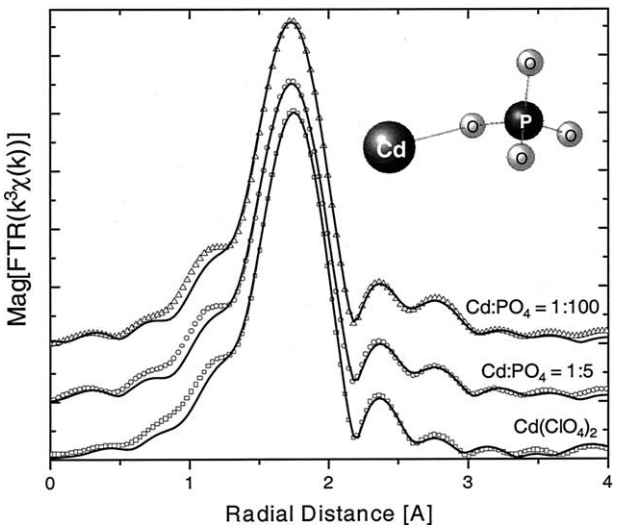

Fig. 3. Data (symbols) and fit (line) for the cadmium perchlorate and phosphate solutions.

Complexation of a Cd atom by acetate molecules decreases the hydration number from 6 to 5 and increases the disorder slightly, as seen by the increase in the O-shell σ^2 value. The C-shell distance we obtain is close to the 2.8 Å determined in crystal $Cd(CH_3COO)_2 0.3H_2O$ (Harrison and Trotter, 1972) and in X-ray scattering studies on solutions with Cd:acetate = 2:4 and Cd:acetate = 1:4 (Caminiti et al., 1984a). The C-shell σ^2 parameter in each of the acetate solutions standards, even though it was unconstrained, converged to similar values, justifying the use of a single σ^2 for a Cd-C interaction, regardless of the number of Cd bound. These results indicate that a Cd-C distance of approximately 2.7 Å is characteristic of an acetate group bound to hydrated Cd.

In summary, the solution standards data provide a qualitative and quantitative understanding of the isolated contribution in the EXAFS spectrum of hydrated Cd, aqueous Cd bound to a carboxyl group, and aqueous Cd bound to a phosphate group.

Table 3. Fit results for the cadmium acetate aqueous solutions.[a]

Shell	N	R(Å)	$\sigma^2(10^{-3}$ Å$^2)$	ΔE_0(eV)
	Cd:Ac = 1:10			
O →	5.9 ± 0.3	2.29 ± 0.01	10.7 ± 0.8	−1.9 ± 0.3
H[b] →	2 × (N_O − 2[c] × N_C)	3.01 ± 0.05	15 ± 10	−1.9 ± 0.3
C →	1.4[d]	2.67 ± 0.03	12 ± 5	−1.9 ± 0.3
CC[e] →	N_c or 2 × N_c	4.24 ± 0.02	14 ± 3	−1.9 ± 0.3
	Cd:Ac = 1:2			
O →	5.9 ± 0.2	2.29 ± 0.01	11.2 ± 0.4	−1.9 ± 0.3
H[b] →	2×(N_O−2[c]× N_C)	3.01 ± 0.06	22 ± 10	−1.9 ± 0.3
C →	1.7[d]	2.67 ± 0.01	10 ± 1	−1.9 ± 0.3
CC[e] →	N_c or 2 × N_c	4.24 ± 0.02	19 ± 2	−1.9 ± 0.3
	Cd:Ac = 1:4			
O →	5.5 ± 0.3	2.30 ± 0.01	11.1 ± 0.7	−0.4 ± 0.3
C →	2.6[d]	2.69 ± 0.01	14 ± 2	−0.4 ± 0.3
CC[e]→	N_c or 2 × N_c	4.27 ± 0.02	20 ± 3	−0.4 ± 0.3
	Cd:Ac = 1:100			
O →	5.1 ± 0.3	2.30 ± 0.01	11.8 ± 0.8	−1.0 ± 0.3
C →	2.9[d]	2.70 ± 0.01	14 ± 2	−1.0 ± 0.3
CC[e]→	N_c or 2 × N_c	4.29 ± 0.03	20 ± 3	−1.0 ± 0.3

[a] Samples are ordered top to bottom by increasing carboxyl binding.
[b] H contribution is not included in the last samples Cd:acetate = 1:4 and 1:100, because it does not contribute significantly to the fit.
[c] Bidentate binding is assumed, whereby the acetate binds with both oxygen atoms, removing two water molecules.
[d] Constrained to values in Table 1.
[e] The number of collinear multiple scattering paths is either N_c or 2 × N_c, depending on the degeneracy of the path.

These models of isolated contributions are used in interpreting the data for the biomass.

3.2. Cd Bound to Biomass: Qualitative Analysis

The edge-step height in fluorescence XAFS spectra is proportional to the total concentration of the element present in the beam, provided that the matrix in which it is embedded and other experimental parameters (e.g., sample geometry, sample thickness, beamline and detector settings) remain unchanged. This feature of XAFS allows comparison of the Cd adsorption in samples of different pH values. Figure 6 shows the edge-step heights as a function of pH. These data show that the Cd concentration in the samples increases with pH, approximately five-fold over the range studied. Comparisons to the edge step heights obtained from solutions of known concentration indicate that Cd concentration is in the mM L^{-1} range. The trend is in general agreement with the model of Fein et al. (1997), although the method used here is less accurate. The biomass concentration in the centrifuged sample paste is not known, and the extent of adsorption should be determined as Cd concentration relative to that of the biomass. All samples were centrifuged the same way so the final biomass concentrations in the

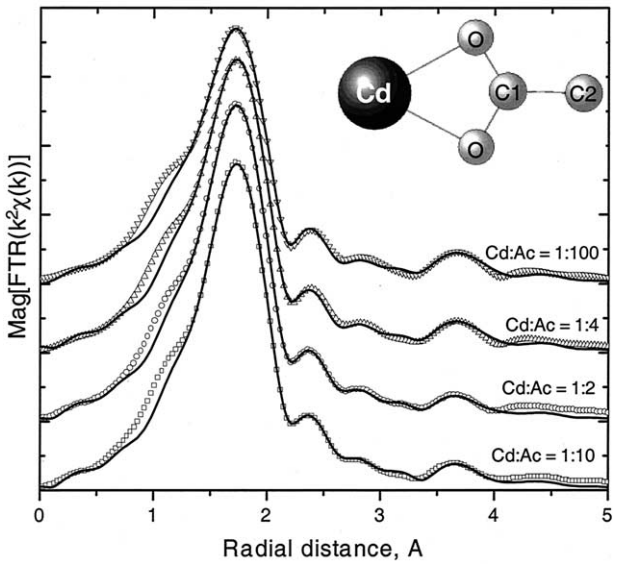

Fig. 5. Data (symbols) and fits (line) for the cadmium acetate solutions.

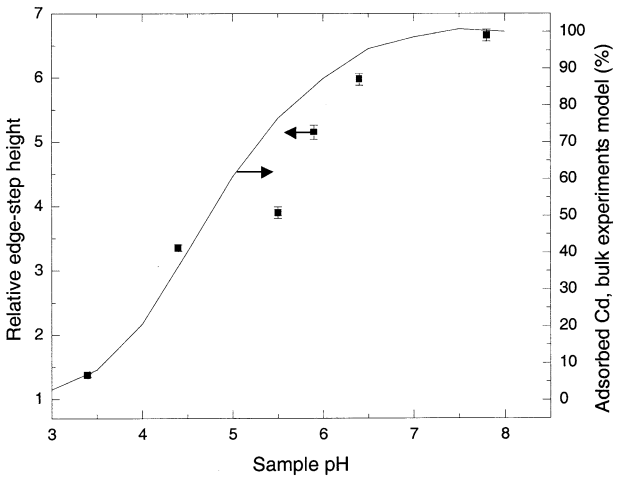

Fig. 6. (square) Edge-step height vs. pH for the biomass samples; (line) normalized bulk adsorption for the current experimental conditions, based on the model in the experiments of Fein et al. (1997). Error bars show the standard deviation of the measurements at four to six beam positions on the samples.

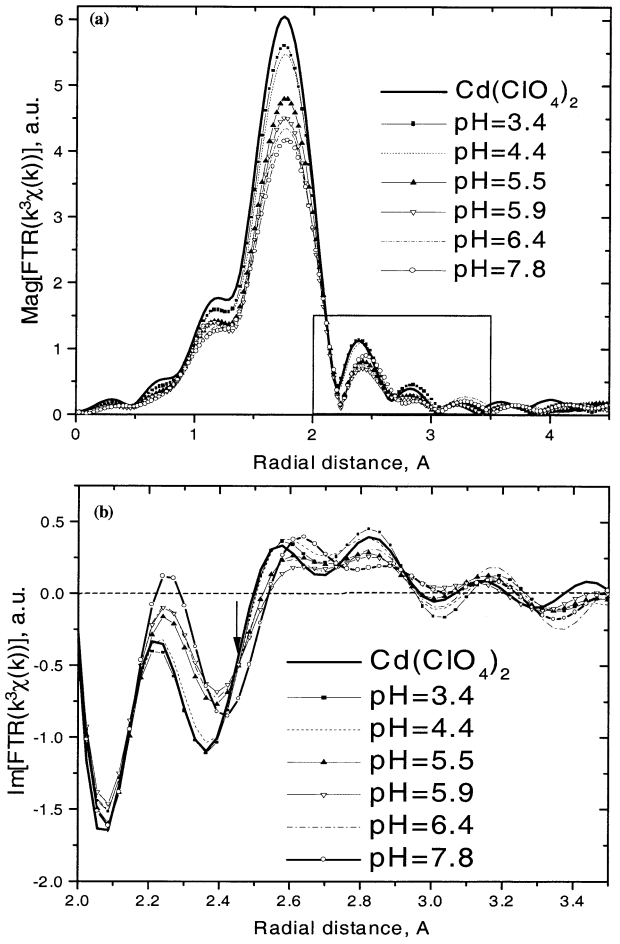

Fig. 7. FT of $[k^3\chi(k)]$ data for all biomass samples (pH 3.4, 4.4, 5.5, 5.9, 6.4, and 7.8). The hydrated cadmium spectrum is included for reference. (a) Magnitude. (b) Imaginary part in the rectangular region shown in (a)

samples are most likely identical; however, differences could in principle be present. In the bulk adsorption experiments where the metal concentration in the supernatants is measured, the control of the initial Cd and biomass concentrations in the suspension is sufficient to determine the amount of Cd adsorbed to the biomass.

The data quality for the biomass samples is illustrated in Figure 1, and Figure 7 shows (a) $|\text{FT } k^3\chi(k)|$ and (b) Im[FT $k^3\chi(k)$] in which the fine differences are observed. The spectrum of the hydrated Cd is also included for reference. Qualitative observation of Figure 7a indicates increasing pH is accompanied by a decrease in amplitude of the first peak, at 1.5 to 2.0 Å in the FT. Spectra for the pH 3.4 and 4.4 samples are quite similar, indicating similar local Cd environments. Compared with the hydrated Cd spectrum, these spectra have smaller first-peak amplitudes and slightly increased amplitudes at 2.8 Å. Similar features are observed for the phosphate solution standards (Fig. 2). This evidence strongly suggests phosphoryl binding in the pH 3.4 and 4.4 samples. Results of the fitting procedure are discussed in the next section.

The next sample in the pH series, at pH 5.5, has a significantly reduced first FT peak amplitude (1.5 to 2.0 Å). Figure 7b indicates larger amplitude at 2.3 Å than in the spectra for hydrated Cd and lower-pH samples. Features are similar to those of the C contribution in the acetate solution spectra (Fig. 4), suggesting that carboxyl binding is significant in controlling Cd adsorption in this sample. Moreover, features become more pronounced at pH 5.9 and 6.4, indicative of increased relative amounts of Cd atoms binding to the carboxyl site. No peaks corresponding to C-C multiple scattering are observed in the biomass spectra, suggesting that the Cd atom, the carboxyl C, and the atom to which this C is attached are not collinear.

The sample at pH 7.8 has a smaller first-peak amplitude than the other biomass samples, and the peak is slightly shifted to higher distance (Fig. 7a). The amplitude of the peak at 2.3 to 2.6 Å is increased relative to that of the mid-pH samples. In the imaginary part of the FT (Fig. 7b), the feature at 2.2 to 2.5 Å has larger amplitude, and its peak-to-peak difference is increased. This was not observed in the mid-pH samples. Finally, all lower-pH samples intersect at the same point (arrow at c.a. 2.5Å), whereas a shift toward a larger distance is observed for pH 7.8. We hypothesize that a contribution from another atom (i.e., binding site) at this distance is mixing with the effect of the carboxyl site already present. The titration data in Fein et al. (1997) and the deprotonation constants of phosphoric acid (Martell and Smith, 1974) suggest that a candidate for a binding site at this pH would be a doubly deprotonated phosphoryl site, HPO_4^{-2}, later modeled with a short-distance P shell labeled P_H. No standard for qualitative comparison could be found.

3.3. Cd Bound to Biomass: Fitting Results and Discussion

On the basis of the qualitative results in the previous section, the following models were used to fit the data from the biomass samples: a hydrated Cd, Cd bound to a carboxyl group, and Cd bound to a phosphoryl ligand, similar to those used in the solution standards fit. Linear combinations of these models were used to represent a mixed binding-site environment.

In all fits, a hydration shell model was first attempted, followed by the addition of a P and/or C shells. Visual improvement of the fit (i.e., elimination of particular misfit in Im[FT $k^n\chi(k)$] by addition of the shell) and a significant reduction in the $\Re$-factor and χ_ν^2 were considered grounds for including the shell in the fit model. For each sample, simultaneous fits of the data were performed at k-weightings of 1, 2, and 3. This was done to reduce the possibility that correlations in the fitting parameters would compensate for a misfit at any single k-weighting and thus increased confidence in the fit model. Because coordination numbers and σ^2 factors are generally correlated when the EXAFS signal is small and the data range is short, a further check of the correctness of the model was a correspondence of obtained σ^2 values with the values in the solution standards or with samples where the Cd local environment is predominantly of one type. Simultaneous fitting of data sets from similar samples was also used to reduce correlations and place common constraints on parameters (e.g., distances and E_0).

The lowest-pH sample, pH 3.4, was successfully fitted with the phosphoryl ligand model, the same model that was fitted to the phosphate solution standards. Fits with a hydration shell model without a phosphoryl ligand (P shell) resulted in a χ_ν^2 value ~2 times larger, and a significant visual misfit was

Table 4. Fit results for the cadmium biomass pH 3.4 sample.

Shell	N	R(Å)	$\sigma^2(10^{-3}$ Å$^2)$	ΔE_0(eV)
O →	5.8 ± 0.2	2.27 ± 0.01	9.3 ± 0.4	−2.2 ± 0.3
H →	2 × (N_O − N_P)	2.91 ± 0.03	11 ± 5	−2.2 ± 0.3
P →	0.8 ± 0.3	3.43 ± 0.03	14 (±5)[a]	−2.2 ± 0.3

[a] σ^2 factor held fixed to the best-fit value in a simultaneous fit of the two phosphate solution standards and the pH 3.4 sample.

present in the region of the P atom, at all three k-weightings. This result excludes the possibility that the Cd left in the sample after centrifugation was predominantly aqueous. We also tested a carboxyl model with a C atom at the distance in the carboxyl ligand. When allowed to vary, the coordination number of such C atoms minimized to zero. Results for the phosphoryl ligand fit are shown in Table 4 and Figure 8. To deal with the correlation between the coordination number and the σ^2 of the P shell, simultaneous fitting of these data and the data from the phosphate solutions was performed, with the σ^2 parameter varying, but equal for all three. Similar values were obtained when all three data sets were fitted independently. By use of this constraint, a common binding mechanism in our solution standards and the biomass is implicitly assumed. This is reasonable if each Cd atom is attached to one biomass ligand. This optimum σ^2 was then used and fixed in the individual data set fits. The final fitting results (Table 4) are similar to those for the phosphate solution standards (Table 2).

The number of P atoms that we calculate to be bound to each Cd atom, 0.8 ± 0.3, supports a metal:ligand stoichiometry of 1:1. Therefore, we conclude that aqueous Cd at pH 3.4 is adsorbed to *B. subtilis* at just one binding site, with structure analogous to the Cd-phosphate solution species. As mentioned before, the speciation of the phosphate solutions could not be determined unequivocally, but a $Cd(H_2O)_{6-x}$ $(OPO_3H_2)_x^{+2-x}$

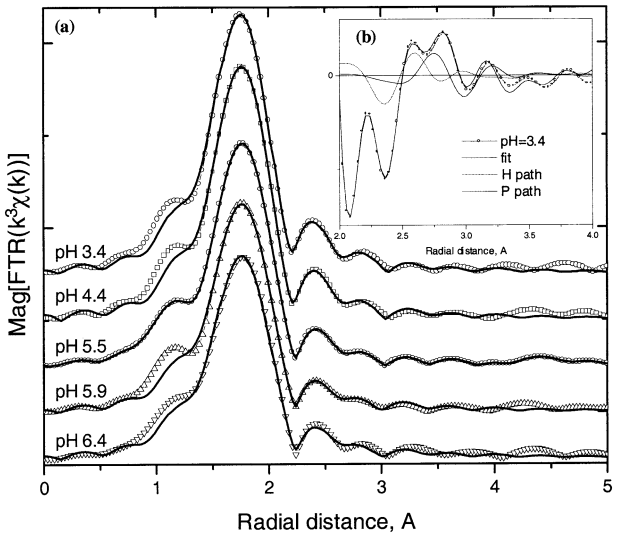

Fig. 8. (a) Magnitude of FT [$k^3\chi(k)$] fits of the pH 3.4, 4.4, 5.5, 5.9, and 6.4 samples. (b) The imaginary part of the pH 3.4 data and fit in the region 2 to 4 Å, showing the contribution from the P atom and lack of significant overlap with the hydration water H atom paths.

species is suggested. The ionization constants (Martell and Smith, 1974) of phosphoric acid, pK_A=2.1 and pK_A=7.2, for removal of one and two hydrogen atoms, respectively, make a diprotic phosphoryl ligand a likely candidate. Recent results on adsorption of a uranyl cation to the same bacterium (Kelly et al., 2001a) also showed that protonated phosphoryl ligands are responsible for the metal complexation at very low pH; that study demonstrated that uranyl adsorption is due to purely phosphoryl binding at pH 1.7, with an increasing carboxyl component to the adsorption in pH 3.2 and pH 4.8 samples.

For our pH 4.4, 5.5, 5.9, and 6.4 biomass samples, the qualitative results indicate an increasing contribution from a carboxyl binding site. This contribution to the EXAFS signal was modeled by addition of a C shell to the pH 3.4 model. For these fits, we assumed that each Cd ion is adsorbed to only one type of ligand (carboxyl or phosphoryl) and that increasing the pH does not change the binding mechanism. Any changes in it (e.g., from monodentate to bidentate or bridged species), would lead to different metal–ligand geometry and should be observed at least as a significant change in distance of the corresponding atom (C, P, etc.). Under these assumptions, parameters of the P shell were held fixed (except for the distance) to the parameters determined in the pH 3.4 fit, and the P-shell contribution at higher pH was weighed by a fraction variable, x_p. The C-shell contribution was weighted by the remainder, $x_c = 1 - x_p$. Correlations caused by the short data range (k = 2.6 to 10.3 Å^{-1}) precluded accurate determination of the coordination number and σ^2 value for this shell from fitting. Fits with the coordination number of C atoms constrained to one and two resulted in overlapping error bars for the fraction parameter x_p. Therefore, the question of Cd:carboxyl stoichiometry cannot be addressed with these data. Fein et al. (1997) obtained better fits to their bulk adsorption data by using a 1:1 metal:ligand stoichiometry when compared with a 1:2 stoichiometry. In the EXAFS fits, we have used this constraint and the number of C atoms in the shell was set to 1.0. Fitting results with a varying C-shell σ^2 parameter are shown in the top half of Table 5. The C-shell σ^2 values for samples at pH 5.5 and 5.9 are similar to those obtained in the standard solutions fits. The results for samples at pH 3.4 and 4.4 are also consistent with the solution standards; however, the amplitude of the C signal is very small, and error bars are correspondingly large. The sample at pH 6.4 displays a sharp drop in C-shell σ^2 value and the fit is of lower quality. This observation becomes more pronounced in the pH 7.8 sample, where this model proves insufficient to fit the data (see below). Thus, the fits at pH 5.5 and 5.9 are assumed to be representative of Cd predominantly bound to a carboxyl biomass ligand, whereas results for the pH 6.4 and 7.8 samples indicate an increase in importance of another binding site. Under our assumption that the carboxyl binding mechanism does not change with pH, the C-shell σ^2 parameter was constrained to the average value found in the samples at pH 5.5 and 5.9, and this constrained model was used to repeat the fitting. This was done to reduce the coordination number-σ^2 correlations (and consequently, error bars) and to make possible a comparison between samples at different pH values in terms of the actual content of the carboxyl and phosphoryl signals. Results for these fits are shown in the bottom part of Table 5, and the quality of the fit is illustrated in Figure 8.

The sample at pH 7.8 is significantly different, as seen from

Table 5. Fit results for the cadmium biomass samples data, pH 3.4 to pH 6.4.

Fitting parameter[a]	pH = 3.4	pH = 4.4	pH = 5.5	pH = 5.9	pH = 6.4
			Floating C shell[b]		
ΔE_0	−2.2 ± 0.6	−1.2 ± 0.5	−1.3 ± 0.5	−1.3 ± 0.5	−1.8 ± 0.8
N_O	5.8 ± 0.2	5.6 ± 0.2	5.2 ± 0.2	4.8 ± 0.2	5.0 ± 0.2
R_O	2.27 ± 0.01	2.28 ± 0.01	2.28 ± 0.01	2.28 ± 0.01	2.27 ± 0.01
σ_O	9.4 ± 0.7	9.2 ± 0.8	9.6 ± 0.6	9.5 ± 0.7	10.6 ± 0.9
R_H	2.91 ± 0.04	2.94 ± 0.04	2.96 ± 0.06	3.00 ± 0.07	2.89 ± 0.07
x_P	0.95 ± 0.25	0.72 ± 0.23	0.32 ± 0.18	0.17 ± 0.19	0.39 ± 0.28
R_P	3.43 ± 0.03	3.43 ± 0.04	3.41 ± 0.08	3.41 ± 0.19	3.45 ± 0.08
R_C	2.71 ± 0.27	2.70 ± 0.13	2.78 ± 0.04	2.76 ± 0.04	2.76 ± 0.03
σ_C	0 ± 65	10 ± 23	11 ± 11	16 ± 11	1 ± 7
			Constrained C shell[b]		
ΔE_0	−2.2 ± 0.4	−1.1 ± 0.5	−1.3 ± 0.3	−1.4 ± 0.4	−1.3 ± 0.6
N_O	5.8 ± 0.2	5.6 ± 0.2	5.1 ± 0.1	4.9 ± 0.1	4.8 ± 0.2
R_O	2.27 ± 0.01	2.28 ± 0.01	2.28 ± 0.01	2.28 ± 0.01	2.28 ± 0.01
σ_O	9.4 ± 0.5	9.1 ± 0.6	9.5 ± 0.4	9.6 ± 0.5	10.0 ± 0.7
R_H	2.91 ± 0.03	2.94 ± 0.03	2.97 ± 0.03	2.99 ± 0.04	2.97 ± 0.05
x_P	0.95 ± 0.19	0.71 ± 0.20	0.31 ± 0.15	0.17 ± 0.15	0.25 ± 0.22
R_P	3.43 ± 0.03	3.43 ± 0.03	3.40 ± 0.07	3.44 ± 0.13	3.42 ± 0.13
R_C	2.75 ± 0.81	2.69 ± 0.13	2.78 ± 0.04	2.76 ± 0.03	2.77 ± 0.05
χ_V^2	36	61	56	13	97
R factor %	0.07	0.07	0.06	0.09	0.22

[a] Units are eV for ΔE, Å for R, and 10^{-3} Å^2 for σ^2.
[b] Fits with varying and constrained σ^2 for the C shell are compared to show that fixing σ^2 does not alter the fit values, but reduces the error bars significantly. σ_C^2 = 0.0135 Å^2 for the constrained fits, as explained in the text.

the qualitative observation of the data. The constrained model used for the lower-pH samples does not adequately fit the pH 7.8 data (Fig. 9) and Table 6, model O+H+C-P). The largest misfit is in the range 2.2 to 3.0 Å. As a starting point, attempts were made to model the data by a hydration shell (O+H), with C or P shells added at the misfit distance. To distinguish this closer P atom from the one in the lower-pH model, it is labeled $P_{7.8}$. Either a C or $P_{7.8}$ shell could separately fit the data, but the numerical results are not realistic and χ_v^2 is about two times larger than for the best fit obtained. In the C-shell fit (Table 6, O+H+C), the C-shell σ^2 value obtained was 0. No such value is seen in the standard solutions or lower-pH samples, and no abrupt change in the carboxyl mechanism of binding is expected for this small change in pH. For the $P_{7.8}$-shell fit (Table 6, O+H+$P_{7.8}$), the σ^2 value obtained was also 0. We could not find a standard to compare this value, but the obtained $P_{7.8}$ number (0.3 ± 0.1) is too small to attribute Cd binding solely to a short-distance phosphoryl ligand. Cd-Cd interactions, as a result of possible polynuclear complex formation or precipitation at this pH, were also considered. The data are inconsistent with Cd-Cd interactions. We conclude that a model consisting of a hydration shell, and a C, $P_{7.8}$, or Cd shells by themselves is not supported by the data.

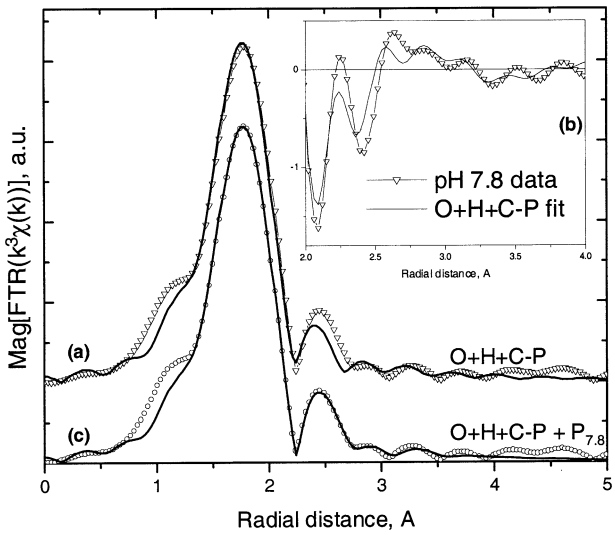

Fig. 9. Magnitude (a) and imaginary part (b) of FT [$k^3\chi(k)$] (triangles) and fit (line) for the pH 7.8 sample, with the model used to fit the low- and mid-pH samples(O+H+C-P). The misfit is clearly seen. (c) Data (circles) and best fit (line) of the pH 7.8 sample, using the constrained O+H+C-P model with an added $P_{7.8}$ shell. Numerical results are in Table 6.

Adding the $P_{7.8}$ shell to the O+H+C-P model used in the lower-pH samples provides the best fit to the pH 7.8 data, with χ_v^2 and $\Re$ factor less than half of those for all other fits (Table 6, model O+H+C-P+$P_{7.8}$). The fit model consists of a hydration shell and a linear combination of a C, P, and $P_{7.8}$ shells, weighed so their total contribution adds up to 1. The parameters for the C and P shells were constrained in the same way as for the lower-pH samples, described above. The parameters for the $P_{7.8}$ shell were allowed to vary freely. The 0.2 coordination number obtained for that shell is interpreted as the Cd being coordinated to one $P_{7.8}$ atom at that binding site, and the site accounting for ~20% of all Cd atoms. The P-shell contribution was weighed by the x_p fraction variable used in the lower pH fits, and the C-shell contribution is weighed by the remainder, $1 - x_p - N_{P\text{-}7.8}$. Results of the fit are shown in Figure 9c and Table 6 (model O+H+C-P+$P_{7.8}$). The fit fraction values for each binding site are as follows: P-shell: 0.33 ± 0.17; C-shell: 0.46 ± 0.19; $P_{7.8}$-shell: 0.21 ± 0.07.

Table 6. Comparison of the fit results for the pH 7.8 sample using different fit models.

Fit model	[a]Ligand atom, L	N_L	R_L(Å)	σ_L^2 (10^{-3} Å^2)	[b]N_H	[c]X_p	χ_v^2	R (%)
O+H+ C−P	—	—	—	—	—	0.03 ± 0.36	129	0.44
O+H+ C	C	0.8 ± 0.9	2.75 ± 0.02	0 ± 9	6 ± 6	—	46	0.11
O+H+ $P_{7.8}$	$P_{7.8}$	0.26 ± 0.13	2.90 ± 0.02	0 ± 4	0 ± 4	—	50	0.14
O+H+ C−P + $P_{7.8}$	$P_{7.8}$	0.21 ± 0.07	2.90 ± 0.01	0 ± 3	0 ± 2	0.33 ± 0.17	21	0.07

[a] This column lists the atom for which information is given in the N_L, R_L, and σ_L columns.
[b] The number of atoms in the H shell is varied while the distance and σ^2 factor are held fixed.
[c] Contribution from the fixed-parameter P shell is weighted by x_p, as in the lower-pH samples fit.

The choice of the shorter distance $P_{7.8}$ shell to compensate the misfit at pH 7.8 requires some justification. In principle, any of the known cell-wall ligands in *B. subtilis* (amino, carboxyl, phosphoryl, hydroxyl) (Beveridge and Murray, 1980) could be responsible for the new binding in the pH 7.8 sample. As mentioned above, the pK_A value for the second deprotonation constant of phosphoric acid is 7.2, making the phosphoryl ligand a likely candidate. Even though XAFS cannot distinguish between atoms at the same distance that have small differences in atomic number (e.g., C/N/O or P/S), it is able to distinguish between atoms in different rows of the periodic table, and the $P_{7.8}$ shell provides a good fit. The C atom does not provide a good fit, which also makes a N-based ligand unlikely. A further constraint on the type of atom is the bond length. On the basis of a tetrahedral PO_4 group of side 2.56 Å and a Cd-O bond length of 2.3 Å, we calculate the maximum Cd-P bond length to be 2.8 Å when both O atoms bind (bidentate) the Cd in the Cd-O-O-P plane. This is close to the determined Cd-$P_{7.8}$ bond length by EXAFS. The small difference could be attributed to a stretched POO< ligand, and/or an increased Cd-O bond length in the bidentate mode. The small σ^2 value is additional evidence for this tight-binding mode. Similarities between the XAFS backscattering functions (F(*k*)) for P and S mentioned above, as well as structural similarities between PO_4 and SO_4 moieties, do not allow the XAFS technique to exclude the possibility of a SO_4-type functional group participating in the Cd sorption in addition to, or in place of, the PO_4 functional group model proposed here. However, the cell wall of *B. subtilis* is rich in phosphoryl binding sites, and no *S*-based analog sites have been identified (Beveridge and Murray, 1980).

Figure 10 shows the relative concentrations of the three different Cd-bacterial surface species that are responsible for the pH dependence of Cd adsorption, according to the proposed EXAFS model. The total concentration of adsorbed Cd is normalized to the extent of adsorption observed at pH 7.8 for comparison purposes. At pH 3.4, Cd-phosphoryl binding dominates the adsorption behavior. Carboxyl ligands account for the majority of the adsorption in the range pH 5.0 to pH 7.8, with the same type of Cd-phosphoryl binding remaining significant throughout this pH range. At pH 7.8, a third binding site becomes available, which accounts for ~20% of the total Cd adsorbed and which is consistent with a shorter distance P bond, possibly from deprotonated phosphoryl sites on the bacterial cell wall similar to HPO_4^{-2} groups.

This speciation model is in general agreement with the surface complexation model proposed by Fein et al. (1997); however, a number of differences exist. Most of the binding in this model and that of Fein et al. (1997) is caused by Cd attachment to deprotonated carboxyl or phosphoryl functional groups, with carboxyl binding increasing in importance from pH 3.4 to 5.9 and short distance (deprotonated) phosphoryl binding becoming important under higher pH conditions. However, the model of Fein et al. (1997) suggests that, under the experimental conditions of this study, attachment of Cd to deprotonated phosphoryl sites should dominate the binding environment of Cd above pH 5.5, and that virtually no Cd-phosphoryl interaction should occur under low pH conditions.

The discrepancy between the extent of deprotonated phosphoryl binding predicted by the model of Fein et al. (1997) compared with our EXAFS data can be ascribed to the relatively large uncertainty associated with the stability constant for Cd-phosphoryl binding reported by Fein et al. (1997). The EXAFS data suggest that the stability constant is significantly lower than the value reported by Fein et al. (1997), with the short Cd-P binding only becoming evident in the pH 7.8 sample. Refinements of Cd-phosphoryl stability constants will be included in a future investigation of metal–phosphoryl binding onto the cell wall of *B. subtilis*.

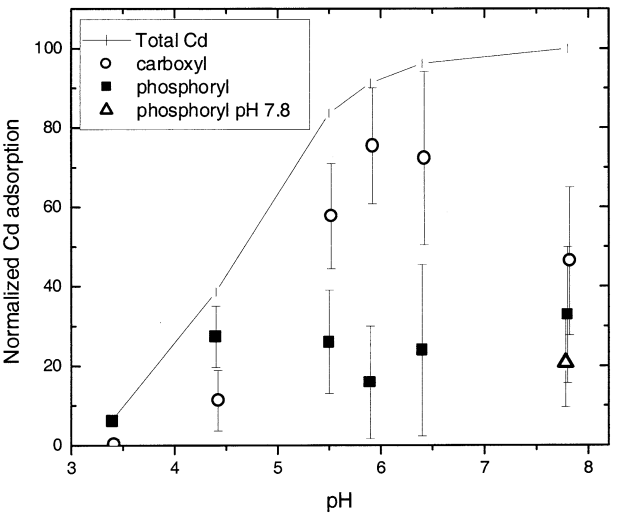

Fig. 10. (solid line) Total Cd adsorption to the biomass according to the model of Fein et al. (1997); (symbols) Cd bound to the different binding sites as a function of pH within the proposed EXAFS model. The data are normalized to the Cd concentration at pH 7.8. Error bars include EXAFS fitting uncertainties and bulk adsorption deviations, added in quadrature.

Fein et al. (1997) modeled the phosphoryl functional group as a site that undergoes a single deprotonation reaction, so that the stoichiometry can be represented as *R*-POH° or *R*-PO^-. In this model, metal attachment only occurs onto the deprotonated species. However, the EXAFS data from this study, along with that of Kelly et al. (2001b) for uranyl-bacteria adsorption, suggest that the phosphoryl site may be more complicated. This study suggests that its chemical behavior is closer to that of aqueous phosphoric acid, with multiple deprotonations possible, and with more than one surface species interacting with adsorbing metal cations. Because little adsorption occurs under low pH conditions in the Cd system, the bulk adsorption data of Fein et al. (1997) could be successfully fitted by ignoring the interactions between Cd and the less-deprotonated phosphoryl site or sites. However, the binding is detectable in the Cd and U EXAFS data, as well as in uranyl bulk adsorption data (Fowle and Fein, 2000). Because of the small amount of adsorption that occurs under these lower pH conditions in the Cd system, such binding could not be detected by using the less sensitive approach of bulk adsorption measurements.

According to the model of Fein et al. (1997), the speciation of the phosphoryl sites remains unchanged between pH 3.4 and 4.4, so the observed increase in adsorption over this pH range could not be ascribed to a corresponding increase in deprotonated phosphoryl sites. The EXAFS data indicate that the low pH binding of Cd is predominantly due to phosphoryl binding. Therefore, this study suggests that the model of Fein et al. (1997) is incomplete, and that another acidity constant for the phosphoryl site exists below the pH range studied by Fein et al. (1997).

4. CONCLUSIONS

Qualitative analysis of the data for the solution standards gives insight into the isolated contributions to the EXAFS from a hydrated Cd ion, a Cd ion bound to a carboxyl group, and a Cd ion bound to a phosphate group. Fits of these standards demonstrate that the ab initio code FEFF8 can model such environments and that the fits place constraints on the correlated structural parameters. On the basis of the analysis of these well-defined standards, we have identified the local environment of Cd adsorbed onto the cell wall of *B. subtilis* and have determined how that environment changes as a function of pH. Very little Cd adsorption to biomass was observed at pH 3.4, and the similarity of the biomass EXAFS data to the phosphate solution standard indicates that Cd is complexed predominantly to groups with similar structure to the aqueous phosphate molecule. As pH increases, a dramatic increase in the amount of Cd bound to the biomass is observed, and the features corresponding to carboxyl binding become more pronounced in the FT. This observation indicates increasing importance of carboxyl binding with increasing pH. Quantitative modeling of the data confirms the qualitative interpretation that binding changes with increasing pH from predominantly phosphoryl to predominantly carboxyl. This analysis also yields quantitative estimates of the Cd:ligand ratios for each ligand, up to pH 6.4.

The spectrum for the biomass sample at pH 7.8 shows a significantly different binding environment compared with that seen for the lower pH samples. Binding to phosphoryl and carboxyl sites cannot account for the EXAFS spectrum observed for the pH 7.8 sample, and binding to a third ligand type must be invoked. This third site is consistent with another type of phosphoryl group, one having a shorter Cd-P distance than that observed for the phosphoryl site present under lower pH conditions. We propose that this third site represents a further deprotonated phosphoryl group, with the shorter Cd-P distance resulting from the bidentate binding to this more electronegative phosphoryl site. The cell-wall structure of *B. subtilis*, the deprotonation constants of phosphoric acid, and the bacterial surface titration data are consistent with the proposed speciation, although an S-bearing ligand cannot be excluded on the basis of the EXAFS data alone.

This study not only provides a detailed understanding of Cd binding to a common type of bacterial surface, but it also illustrates that EXAFS spectroscopy is ideally suited to complement bulk adsorption measurements in constructing quantitative models of adsorption of metals onto bacteria. XAFS provides detailed information concerning the binding environment of the metal of interest, whereas bulk adsorption measurements can be used to constrain the values of the thermodynamic stability constants for the important metal–bacterial surface complexes. Taken together, bulk adsorption measurements and XAFS experiments represent a powerful approach for determining and modeling metal speciation and distribution in microbe–water–mineral systems.

Acknowledgments—M.B. thanks the Bayer Corporation for its support through the Bayer Predoctoral Fellowship in Environmental Science. Beamline setup help from the staff of MRCAT is greatly appreciated. We thank associate editor David J. Wesolowski and three anonymous reviewers for comments that significantly improved the manuscript. This work was supported in part by NSF grant EAR99-05704 and the U.S. Department of Energy, Office of Science, Office of Biologic and Environmental Research, NABIR program. MR-CAT is supported by the U.S. Department of Energy under contract DE-FG02-94-ER45525 and the member institutions. Use of the Advanced Photon Source was supported by the U.S. Department of Energy under contract W-31-109-Eng-38.

Associate editor: D. Wesolowski

REFERENCES

Ankudinov A. L., Ravel B., Rehr J. J., and Conradson S. D. (1998) Real-space multiple-scattering calculation and interpretation of X-ray absorption near-edge structure. *Phys. Rev. B* **58,** 7565–7576.

Averbuch-Pouchot M. T., Durif A., Guitel J. C., Tordjman I., and Laugt M. (1973) Crystal structure of $Cd(H_2PO_4)2 \cdot H_2O$. *Bull. Soc. Fr. Mineral. Christallogr.* **96,** 278–280.

Baes C. F. and Mesmer R. E. (1973) *Hydrolysis of Cations*. Wiley.

Bethke C. M. and Brady P. V. (2000) How the K-d approach undermines ground water cleanup. *Ground Water* **38,** 435–443.

Beveridge T. J. and Murray R. G. E. (1976) Uptake and retention of metals by cell-walls of Bacillus subtilis. *J. Bacteriol.* **127,** 1502–1518.

Beveridge T. J. and Murray R. G. E. (1980) Sites of metal deposition in the cell wall of Bacillus subtilis. *J. Bacteriol.* **141,** 876–887.

Beveridge T. J. and Koval S. F. (1981) Binding of metals to cell envelopes of Escherichia coli K-12. *Appl. Environ. Microbiol.* **42,** 325–335.

Bigi A., Foresti E. B., Gazzano M., Ripamonti A., and Roveri N. (1986) Cadmium-substituted tricalcium phosphate and crystal structure refinement of beta'-tricadmium phosphate. *J. Chem. Res* **5**(S), 170–171.

Brown G. E. (1990) Spectroscopic studies of chemisorption reaction mechanisms at oxide-water interfaces. In *Mineral–Water Interface Geochemistry,* Vol. 23 (eds. M. F. Hochella and A. F. White), pp.

309–363. Reviews in Mineralogy. Mineralogical Society of America.

Caminiti R. (1982) Nickel and cadmium phosphates in aqueous solution—Cation-anion complex formation and phosphate-H2O interactions. *J. Chem. Phys.* **77,** 5682–5686.

Caminiti R. and Johansson G. (1981) On the structures of cadmium sulfate complexes in aqueous solutions. *Acta Chem. Scand., Ser. A* **35,** 373–381.

Caminiti R., Cucca P., Monduzzi M., Saba G., and Crisponi G. (1984a) Divalent metal–acetate complexes in concentrated aqueous solutions—An X-ray diffraction and NMR spectroscopy study. *J. Chem. Phys.* **81,** 543–551.

Caminiti R., Cucca P., and Radnai T. (1984b) Investigation on the structure of cadmium nitrate aqueous solutions by X-ray diffraction and Raman spectroscopy. *J. Phys. Chem.* **88,** 2382–2386.

Collins C. R., Ragnarsdottir K. V., and Sherman D. M. (1999) Effect of inorganic and organic ligands on the mechanism of cadmium sorption to goethite. *Geochim. Cosmochim. Acta* **63,** 2989–3002.

Crist R. H., Oberholser K., Shank N., and Nguyen M. (1981) Nature of bonding between metallic ions and algal cell-walls. *Environ. Sci. Technol.* **15,** 1212–1217.

Farquhar M. L., Vaughan D. J., Hughes C. R., Charnock J. M., and England K. E. R. (1997) Experimental studies of the interaction of aqueous metal cations with mineral substrates: Lead, cadmium, and copper with perthitic feldspar, muscovite, and biotite. *Geochim. Cosmochim. Acta* **61,** 3051–3064.

Fein J. B. (2000) Quantifying the effects of bacteria on adsorption reactions in water-rock systems. *Chem. Geol.* **169,** 265–280.

Fein J. B., Daughney C. J., Yee N., and Davis T. A. (1997) A chemical equilibrium model for metal adsorption onto bacterial surfaces. *Geochim. Cosmochim. Acta* **61,** 3319–3328.

Fein J. B., Martin A. M., and Wightman P. G. (2001) Metal adsorption onto bacterial surfaces: Development of a predictive approach. *Geochim. Cosmochim. Acta* **65,** 4267–4273.

Fowle D. A. and Fein J. B. (2000) Experimental measurements of the reversibility of metal–bacteria adsorption reactions. *Chem. Geol.* **168,** 27–36.

Goncalves M. D. S., Sigg L., Reutlinger M., and Stumm W. (1987) Metal–ion binding by biological surfaces—Voltammetric assessment in the presence of bacteria. *Sci. Total Environ.* **60,** 105–119.

Harrison W. Trotter J. (1972) Crystal and molecular structure of cadmium diacetate dihydrate. J. Chem. Soc. Dalton Trans. 956–960.

Harvey R. W. and Leckie J. O. (1985) Sorption of lead onto two gram-negative marine bacteria in seawater. *Mar. Chem.* **15,** 333–344.

Hennig C., Panak P. J., Reich T., Rosberg A., Raff J., Selenska-Pobell S., Matz W., Bucher J. J., Bernhard G., and Nitsche H. (2001) EXAFS investigation of uranium(VI) complexes formed at. *Bacillus cereus and Bacillus sphaericus surfaces. Radiochim. Acta* **89,** 625–631.

Kelly S. D., Boyanov M. I., Bunker B. A., Fein J. B., Fowle D. A., Yee N., and Kemner K. M. (2001a) XAFS determination of the bacterial cell wall functional groups responsible for complexation of Cd and U as a function of pH. *J. Synchrot. Radiat.* **8,** 946 –948 .

Kelly S. D., Kemner K. M., Fein J. B., Fowle D. A., Boyanov M. I., Bunker B. A., and Yee N. (2002) X-ray absorption fine structure determination of pH-dependent U-bacterial cell wall interactions. *Geochim. Cosmochim. Acta* **66**(2)**,** 3855–3871.

Kemner K. M., Kropf J., and Bunker B. A. (1994) A low-temperature total electron yield detector for X-ray absorption fine-structure spectra. *Rev. Sci. Instrum.* **65,** 3667–3669.

Konhauser K. O., Fyfe W. S., Ferris F. G., and Beveridge T. J. (1993) Metal sorption and mineral precipitation by bacteria in two Amazonian river systems—Rio-Solimoes and Rio-Negro, Brazil. *Geology* **21,** 1103–1106.

Koningsberger D. C. and Prins R. (1988) *X-ray Absorption: Principles, Applications, Techniques of EXAFS, SEXAFS, and XANES*. Wiley.

Koretsky C. (2000) The significance of surface complexation reactions in hydrologic systems: A geochemist's perspective. *J. Hydrol.* **230,** 127–171.

Kramer U., Cotter–Howells J. D., Charnock J. M., Baker A. J. M., and Smith J. A. C. (1996) Free histidine as a metal chelator in plants that accumulate nickel. *Nature* **379**(6566), 635–638.

Marcus Y. (1988) Ionic radii in aqueous solutions. *Chem. Rev.* **88,** 1475–1498.

Martell A. E. and Smith R. M. (1974) *Critical Stability Constants*. Plenum Press.

Martinez R. E. and Ferris F. G. (2001) Chemical equilibrium modeling: Techniques for the analysis of high-resolution bacterial metal sorption data. *J. Colloid Interface Sci.* **243,** 73–80.

Newville M., Livins P., Yacoby Y., Rehr J. J., and Stern E. A. (1993) Near-edge X-ray absorption fine structure of Pb—A comparison of theory and experiment. *Phys. Rev. B* **47,** 14126–14131.

Newville M., Ravel B., Haskel D., Rehr J. J., Stern E. A., and Yacoby Y. (1995) Analysis of multiple-scattering XAFS data using theoretical standards. *Physica B* **208–209,** 154–156.

O'Day P. A. (1999) Molecular environmental geochemistry. *Rev. Geophys.* **37,** 249–274.

O'Day P. A., Carroll S. A., and Waychunas G. A. (1998) Rock-water interactions controlling zinc, cadmium, and lead concentrations in surface waters and sediments, US Tri-State Mining District. 1. Molecular identification using X-ray absorption spectroscopy. *Environ. Sci. Technol.* **32,** 943–955.

Ohtaki H., Maeda M., and Ito S. (1974) X-ray diffraction studies of aqueous solutions of cadmium perchlorate and sodium tetraiodocadmate. *Bull. Chem. Soc. Jpn.* **47,** 2217–2221.

Ohtaki H. and Radnai T. (1993) Structure and dynamics of hydrated ions. *Chem. Rev.* **93,** 1157–1204.

Panak P. J., Raff J., Selenska-Pobell S., Geipel G., Bernhard G., and Nitsche H. (2000) Complex formation of U(VI) with *Bacillus*isolates from a uranium mining waste pile. *Radiochim. Acta* **88,** 71–76.

Panak P. J., Booth C. H., Caulder D. L., Bucher J. J., Shuh D. K., and Nitsche H. (2002) X-ray absorption fine structure spectroscopy of plutonium complexes with bacillus sphaericus. *Radiochim. Acta* **90,** 315–321.

Randall S. R., Sherman D. M., Ragnarsdottir K. V., and Collins C. R. (1999) The mechanism of cadmium surface complexation on iron oxyhydroxide minerals. *Geochim. Cosmochim. Acta* **63,** 2971–2987.

Ravel B. (2001) ATOMS: Crystallography for the X-ray absorption spectroscopist. *J. Synchrot. Radiat.* **8,** 314–316.

Salt D. E., Prince R. C., Pickering I. J., and Raskin I. (1995) Mechanisms of cadmium mobility and accumulation in Indian mustard. *Plant Physiol.* **109,** 1427–1433.

Salt D. E., Pickering I. J., Prince R. C., Gleba D., Dushenkov S., Smith R. D., and Raskin I. (1997) Metal accumulation by aquacultured seedlings of Indian mustard. *Environ. Sci. Technol.* **31,** 1636–1644.

Sarret G., Manceau A., Cuny D., Van Haluwyn C., Deruelle S., Hazemann J. L., Soldo Y., Eybert-Berard L., and Menthonnex J. J. (1998a) Mechanisms of lichen resistance to metallic pollution. *Environ. Sci. Technol.* **32,** 3325–3330.

Sarret G., Manceau A., Spadini L., Roux J. C., Hazemann J. L., Soldo Y., Eybert-Berard L., and Menthonnex J. J. (1998b) Structural determination of Zn and Pb binding sites in Penicillium chrysogenum cell walls by EXAFS spectroscopy. *Environ. Sci. Technol.* **32,** 1648–1655.

Sarret G., Vangronsveld J., Manceau A., Musso M., D'Haen J., Menthonnex J. J., and Hazemann J. L. (2001) Accumulation forms of Zn and Pb in Phaseolus vulgaris in the presence and absence of EDTA. *Environ. Sci. Technol.* **35,** 2854–2859.

Segre C. U., Leyarovska N. E., Chapman L. D., Lavender W. M., Plag P. W., King A. S., Kropf A. J., Bunker B. A., Kemner K. M., Dutta P., Duran R. S., and Kaduk J. (2000) The MRCAT insertion device beamline at the Advanced Photon Source. In *Synchrotron Radiation Instrumentation: Eleventh U.S. National Conference* (ed. P. Pianetta), pp. 419–422. CP521. American Institute of Physics.

Sery A., Manceau A., and Greaves G. N. (1996) Chemical state of Cd in apatite phosphate ores as determined by EXAFS spectroscopy. *Am. Miner.* **81,** 864–873.

Sillen L. D. and Martell A. E. (1964) *Stability Constants*. Special Publication No. 17. Chemical Society, London.

Sillen L. D. and Martell A. E. (1971) *Stability Constants*. Supplement No. 1, Special Publication No. 25. Chemical Society, London.

Spadini L., Manceau A., Schindler P. W., and Charlet L. (1994) Structure and stability of Cd2+ surface complexes on ferric oxides. 1. Results from EXAFS spectroscopy. *J. Colloid Interface Sci.* **168,** 73–86.

Stern E. A. and Heald S. M. (1979) X-ray filter assembly for fluorescence measurements of X-ray absorption fine structure. *Rev. Sci. Instrum.* **50,** 1579–1582.

Stern E. A. and Heald S. M. (1983) Basic principles and applications of EXAFS. In *Handbook of Synchrotron Radiation* (ed. E. E. Koch), pp. 995–1014. Elsevier.

Stern E. A., Newville M., Ravel B., Yacoby Y., and Haskel D. (1995) The UWXAFS analysis package—philosophy and details. *Physica B* **209,** 117–120.

Venema P., Hiemstra T., and van Riemsdijk W. H. (1996) Multisite adsorption of cadmium on goethite. *J. Colloid Interface Sci.* **183,** 515–527.

Warren L. A. and Haack E. A. (2001) Biogeochemical controls on metal behaviour in freshwater environments. *Earth-Sci. Rev.* **54,** 261–320.

Webb S. M., Gaillard J. F., Jackson B. E., and Stahl D. A. (2001) An EXAFS study of zinc coordination in microbial cells. *J. Synchrot. Radiat.* **8,** 943–945.

Xia K., Bleam W., and Helmke P. A. (1997a) Studies of the nature of binding sites of first row transition elements bound to aquatic and soil humic substances using X-ray absorption spectroscopy. *Geochim. Cosmochim. Acta* **61,** 2223–2235.

Xia K., Bleam W., and Helmke P. A. (1997b) Studies of the nature of Cu^{2+} and Pb^{2+} binding sites in soil humic substances using X-ray absorption spectroscopy. *Geochim. Cosmochim. Acta* **61,** 2211–2221.

Xia K., Weesner F., Bleam W. F., Bloom P. R., Skyllberg U. L., and Helmke P. A. (1998) XANES studies of oxidation states of sulfur in aquatic and soil humic substances. *Soil Sci. Soc. Am. J.* **62,** 1240–1246.

Xia K., Skyllberg U. L., Bleam W. F., Bloom P. R., Nater E. A., and Helmke P. A. (1999) X-ray absorption spectroscopic evidence for the complexation of Hg(II) by reduced sulfur in soil humic substances. *Environ. Sci. Technol.* **33,** 257–261.